Advanced real-time digital microscopy of foaming processes

MARKUS HONKANEN AND HANNU ELORANTA

ABSTRACT: The properties of aqueous foams play a major role in foam forming and foam coating. Inline real-time foam measurements provide highly desired opportunities for optimization and control of foaming processes.

This paper presents inline digital microscopy measurements of aqueous foams in foaming processes. It presents methods for providing detailed information on foam quality parameters, such as foam density and foam homogeneity in real time from the process. In addition, this study evaluates the performance of transillumination and front-light illumination in imaging of foams. The tests show very good results for the transillumination approach. Limitations of the image-based optical technique are discussed, and the precision of bubble size distribution measurement is assessed with a certificated reference substance. The measured foam densities are compared against the reference foam densities in the range 100–300 g/L, providing a linear correlation with R^2 value of 0.99. In the case of heterogenous foams with a wide bubble size distribution, the bubble size-dependent dimensionless depth of field must be taken into account to obtain accurate estimates of foam density. Bubble-scale foam homogeneity is described by the standard deviation of bubble size distribution in foam.

Application: This study quantifies the accuracy of digital microscopy in measuring foam bubble size distribution and its standard deviation (i.e., foam homogeneity in bubble scale) and foam density directly from the foam process. It highlights the difference in front light and transillumination approaches and helps the reader in designing the right type of system for the application.

The control of gas dispersion properties plays an important role in many processes in the pulp and paper industry; examples include pulp delignification, foam coating, and foam forming. Inline monitoring of foam bubble size, shape, and foam density enable optimization and troubleshooting of the foaming process. Real-time diagnostics allow instant detection of sudden changes in the operational parameters of the process. Examples of such the studies in the pulp and paper industry are presented in [1-4].

Foam is a compressible substance whose properties constantly change during the foaming process. Foam compressibility plays a major role when foam is generated at high pressure and dispensed to ambient pressure. The size of foam bubbles changes with pressure and temperature based on the ideal gas law. For a given mole amount of ideal gas, the ideal gas law states that the gas pressure times the gas volume is constant in an isothermal process. Gas volume inside each gas bubble decreases linearly with increasing the pressure. Consequently, bubble diameter decreases as a ratio of a pressure ratio term raised to the 1/3 power:

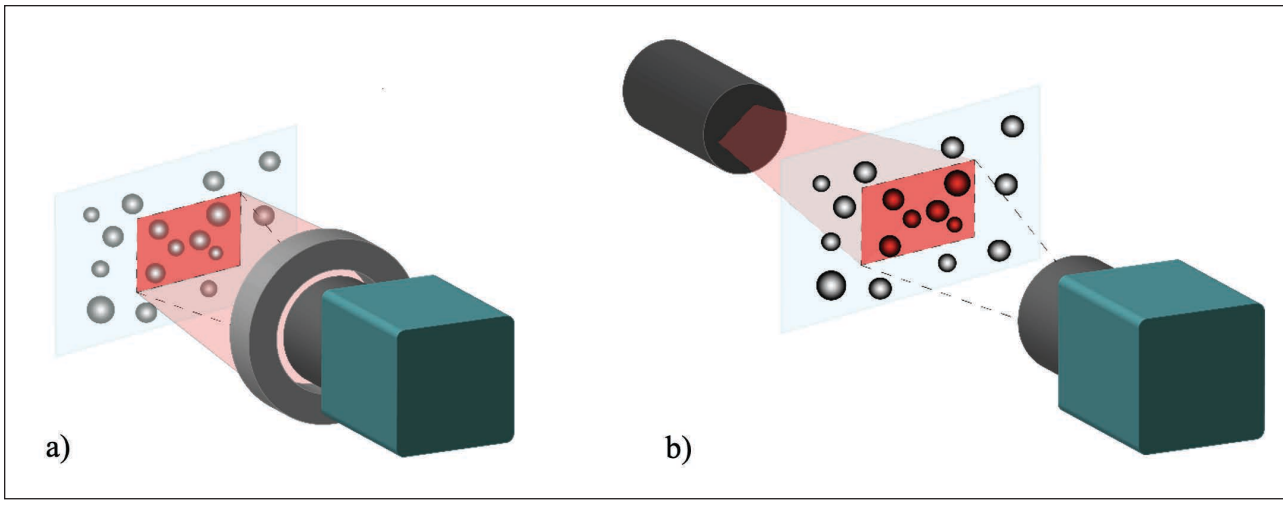
$$d_{fp} = d_0 \left(\frac{p_0}{p_{fp}}\right)^{1/3} \quad (1)$$

where d_{fp} is the bubble diameter in the foaming process in absolute pressure p_{fp}. Equation 1 derives d_{fp} estimate based on the process pressure and the bubble diameter d_0 measured at the process outlet at ambient pressure p_0 (101.325 kPa). Similarly, foam density in the foaming process ρ_{fp} can be estimated weighing a foam sample at ambient pressure with a digital scale and converting the result to process pressure:

$$\rho_{fp} = \frac{\rho_0 \cdot \rho_l}{\rho_0 + \frac{p_0}{p_{fp}}(\rho_l - \rho_0)} \quad (2)$$

where ρ_0 is the reference foam density at ambient pressure (p_0), ρ_l is liquid density, and p_{fp} is the absolute pressure in the process. The pressure scaling does not take account of bubble coalescence rate and drainage in the process line; it assumes stable foam with a great longevity. For that reason, the pressure scaling-based predictions may overestimate the gas bubble size and underestimate the foam density in the process.

Based on our experiences with foaming processes, foams are highly sensitive to fluid dynamic forces. The elongation of gas bubbles due to fluid dynamic forces increases their surface area, increasing their tendency to coalesce with neighboring bubbles. The lighter the foam is, the more carefully it must be processed. In addition to foam density, bubble size is an important property of foam [1]. Heterogenous bubble size distribution increases coalescence rate, because bubbles of different sizes introduce



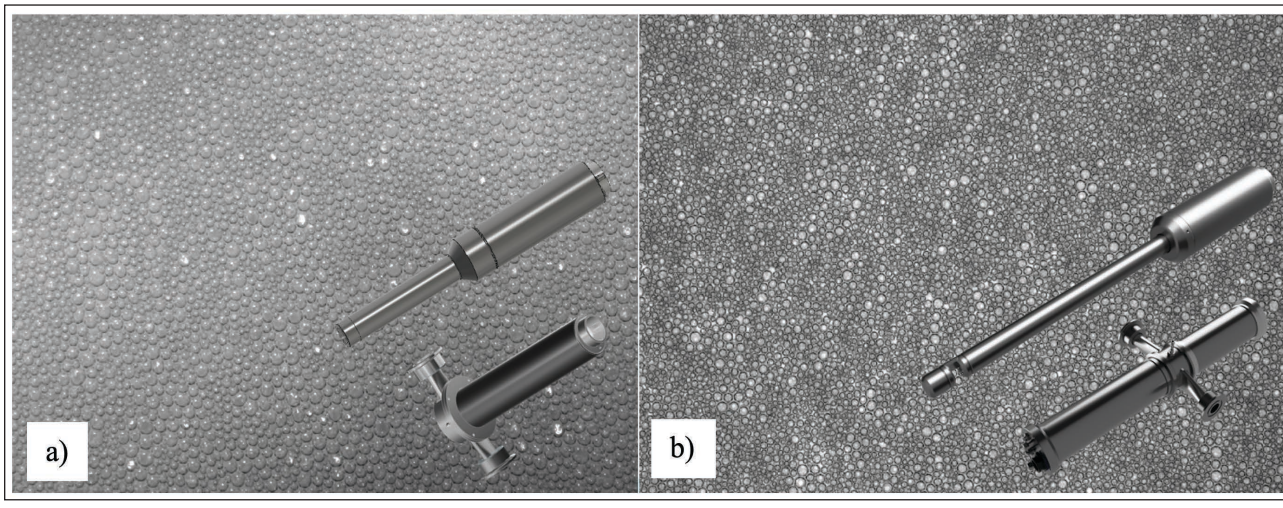
1. Sketches of a) front light and b) transillumination (back light) camera arrangements for foam inspection.

relative velocity between each other. The heterogeneity of the generated bubble size distribution increases with time, and it cannot be compensated later in the process. Foam stability increases as both the mean bubble size and the standard deviation of bubble size decrease, and at the same time, foam becomes more resistant against fluid dynamic forces.

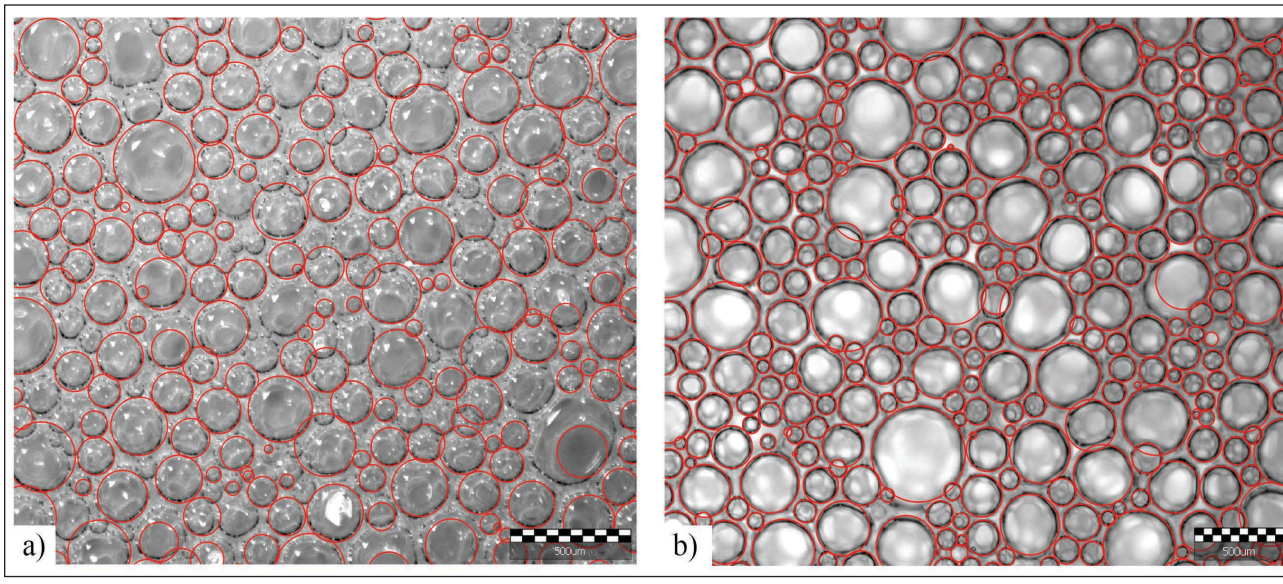
Camera-based measurements of bubble size distribution have already been introduced in the era of analog cameras. In the 1980s, Kroezen et al. [5,6] measured bubble size distributions in the foaming process via manual bubble size measurement from the photographs of foam captured through a sight glass. They addressed multiple sources of error in the image-based measurement of bubble size distribution. The same sources of error are also addressed in this study. Camera-based measurements are limited to the surface layer, because the light rays from target to camera sensor become distorted and blurred when they travel through substances with varying refractive indices. In the case of foams, this corresponds to the first layer of bubbles in the close vicinity of the viewing window or sight glass. The validation measurements of this study will reveal how these limitations affect the accuracy of the measures.

MEASUREMENT METHOD

Commercial camera-based measurement systems are utilized in this study. Systems capture sharp images of fast-moving foam bubbles in a micron scale resolution (3 µm/pixel) utilizing a digital machine vision camera equipped with a telecentric measuring lens and high-power strobe lighting. The developed software automatically detects bubbles in foam images, measures their projected areas, and reports the measured statistics in the software user interface in real time. Systems are intended to study aqueous foams, with a foam bubble size range from 10 µm to 3 mm in diameter. Foam bubbles can be illuminated either from the front or from behind (transillumination). Measurement setups of both approaches are presented in **Fig. 1**. The light blue layer in the sketch presents the studied suspension. In the front light setup (Fig. 1a), the camera is equipped with a ring light directed towards the foam. In the transillumination setup (Fig. 1b), a spotlight is located



2. Imaging probes and their foam images: a) front light illumination type, and b) transillumination type.



3. Closeups of a) front light illuminated image, and b) transilluminated image where the bubble detections are circled.

on the opposite side of the foam and directed towards the camera. Transillumination requires two viewing windows into the foam suspension with a relatively narrow distance (3 mm in this study), whereas the front illumination setup enables multiple installation options and a blockage-free approach for high consistency pulp foam suspensions.

Figure 2 shows example images of the same foam captured by a front light imaging probe (Fig. 2a) and a transillumination imaging probe (Fig. 2b). The imaging probes are shown in Fig. 2 on top of their foam images. There are imaging probes for reactors and flow-through imaging cells for pipelines. The transillumination type produces reflection-free high-contrast images of foam bubbles, where the dark silhouettes correspond to the outlines of bubbles, enabling accurate sizing of gas bubbles. The front light illumination method cannot match the image quality of the transillumination method, but bubbles can be recognized from the front illuminated images (Fig. 2a).

Why do we choose the front light illumination for some applications, even though the transillumination approach produces better image quality?

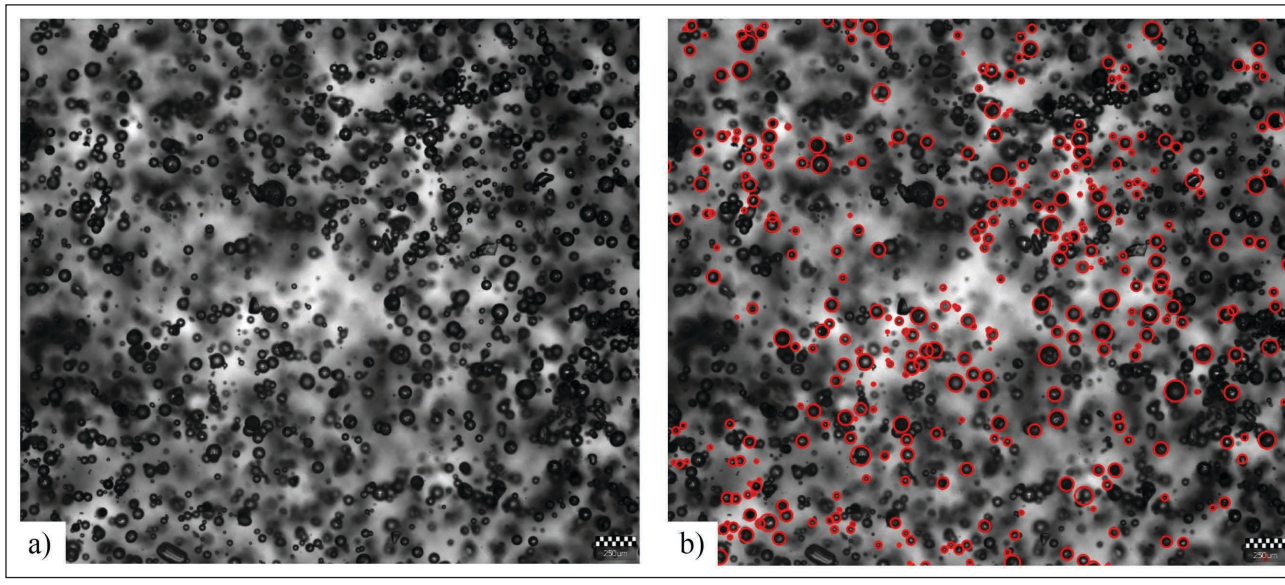
1) Front light illumination can be utilized for pigmented foams, whose light transmittance is low, and for high-consistency pulp foams, in which fiber flocs could block the thin measurement cap of a transillumination probe.
2) Object color can be measured from reflected light utilizing a white light source.
3) The front light method enables an easy installation in the process; suspension can be studied through a reactor sight glass [7] or through a valve [3,4]. Non-intrusive foam measurements are possible with front light illumination.

The developed automatic image analysis algorithm detects all gas bubbles in an image and measures their diameters in less than a second per image. The area fractions of gas and liquid phases in an image are calculated by detecting all gas bubbles that appear sharp in an image [8]. Those bubbles are located inside the depth of field of the imaging system. The bubbles located outside the focal plane appear blurry in the image, and they are discarded from analysis.

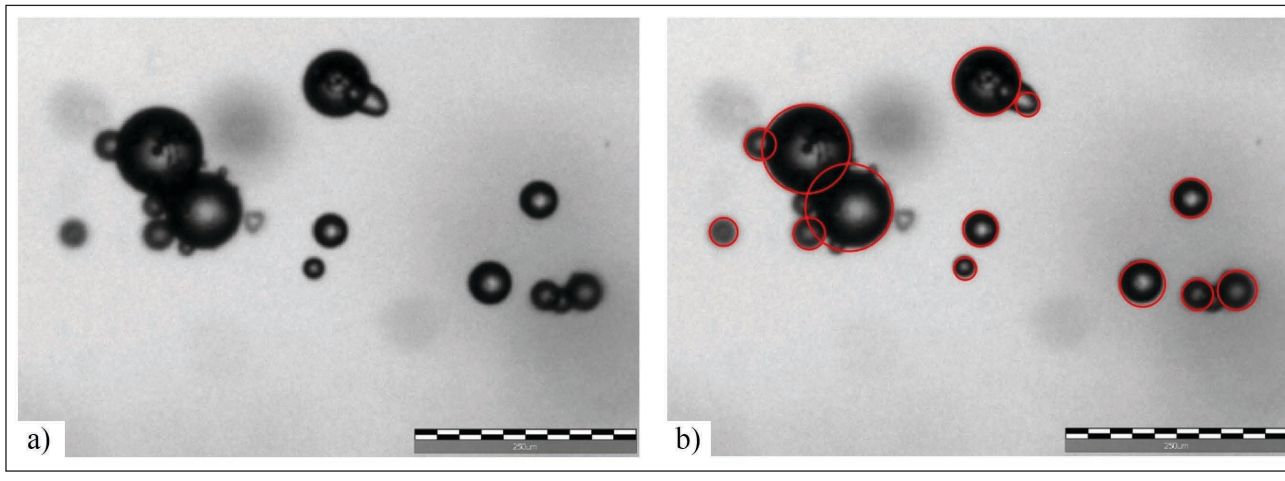
Gas bubbles appear as dark rings on a bright background. Rings are detected with an iterative least squares circle fit. The bubble size is determined equal to the diameter of the circle fitted on it. To locate a valid gas bubble, at least 60% of its ring outline needs to be visible in the image inside the bubble-size adaptive radius range. Gas bubbles can have more irregular shape in the validation phase. The precision of the bubble size measurement obviously decreases with increasing the deformation of bubbles.

Figure 3 shows closeup images of a front light-illuminated foam image (Fig. 3a) and a transilluminated foam image (Fig. 3b) where the bubble detections are shown with red circles. Most of the detection circles correspond very well to the bubble outlines. Some bubbles in the front light-illuminated image remain undetected. Tiny glare points on top of bubble outlines disturb the bubble detection algorithm. Nevertheless, the detection circles seem to represent the size distribution of foam bubbles very well for the front-light illuminated image also.

Foam density measurement would be a highly beneficial feature for an inline process microscopy system that monitors foam quality in real time in the process line. Density estimation with a planar 2D measurement technique is obviously a challenge. However, it has been shown that by measuring an arbitrary projected area fraction, an unbiased estimate of the volume fraction can be obtained [9]. In 2005, Overby and Johnson presented a model to back-project the



4. a) Transilluminated image of certificated glass beads, and b) the same image where the detections are circled.



5. a) Closeup of a transilluminated image of glass beads, and b) the same image where the detections are circled.

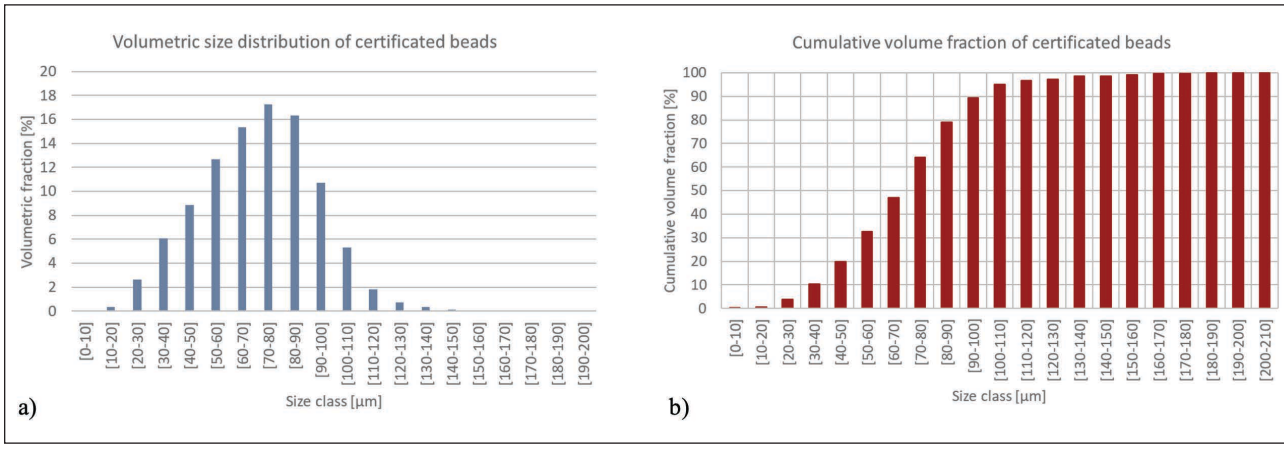
3D properties from 2D perspective projections of micrographs [9]. They presented that the ratio of the 2D projected area fraction and the 3D volume fraction is an exponential function of the dimensionless depth of field, τ:

$$\frac{1-A_A'}{1-V_V} = \exp\left[-\tau\right], \quad (3)$$

where V_V is the gas void fraction, A_A' is projected area fraction of gas bubbles and the dimensionless depth of field $\tau = \frac{tS_V}{4(1-V_V)}$, where t is the depth of field in image and S_V is the gas-liquid surface area in the volume, which can be approximated $S_V = \frac{6 \cdot V_V}{d_{32}}$, where d_{32} is Sauter mean diameter of bubbles. This gives $\tau = \frac{3 \cdot t \cdot V_V}{2 \cdot d_{32(1-V_V)}}$. The derivation of Eq. 3 assumes that bubbles are evenly distributed in suspension and that all bubbles are non-interpenetrating, spherical, and of the same size. That is mostly not the case for industrial foams. However, Eq. 3 highlights the issue with the depth dimension of the measurement: the effective depth of field is a function of gas void fraction and bubble size. Larger bubbles are detected with a larger depth range. At high gas void fractions, the effective depth of field reduces to the scale of the bubble radius, whereas at low void fraction, bubbles deeper in suspension can be detected in the image. This study addresses these challenges and shows the performance of foam density measurement with respect to foam homogeneity.

ACCURACY ASSESSMENT OF BUBBLE SIZE MEASUREMENT

Accuracy assessment of gas bubble size measurement has been carried out with Malvern Panalytical's Quality Audit Standard QAS4002 Measurement Protocols 2.5 g one-shot polydisperse glass bead transfer standard [10]. Calibrated glass beads are generally utilized for accuracy assessments of particle, bubble, and droplet analyzers (e.g., [8,11]). The transillumination probe is utilized in the accuracy assess-



6. a) Normalized volumetric size distribution of certificated glass beads measured with transillumination probe, and b) the same distribution in cumulative form (to read the 10-%, 50-% and 90-% percentile values from the graph).

ment. **Figure 4** shows an image with lots of glass beads and the same image with detections overlaid on top of the image. Images of glass beads have higher contrast than images of foam. The concentration of glass beads is relatively low, so we can recognize blurred, out-of-focus beads located outside the 200 µm thin depth of field. Those beads are rejected based on the focus discrimination procedure of the detection algorithm. A closeup image of glass beads is shown in **Fig. 5**. Visual observation shows that circular detections correspond to the outlines of glass beads quite well, although most of the beads appear to overlap with each other in the captured images.

Table I presents both the reference values and measured values of the 10-%, 50-%, and 90-% level diameters of the volumetric size distribution of certificated glass beads. Assessment shows that the transillumination-based imaging system measures the glass bead size distribution within the reference range of the certificated substance. The measured size distribution is shown in **Fig. 6** in volume frequency (Fig. 6a) and cumulative volume fraction form (Fig. 6b). The 10-% and 90-% percentile values of the measured cumulative volume distribution are closer to each other than the reference target values, although all values are within the reference range. We are not sure whether the properties of the measured sample match our measures precisely or whether our measures underestimate the quantities of very small beads and very large beads. We can visually observe some irregularly-shaped large glass beads, which are rejected by the bubble detection algorithm.

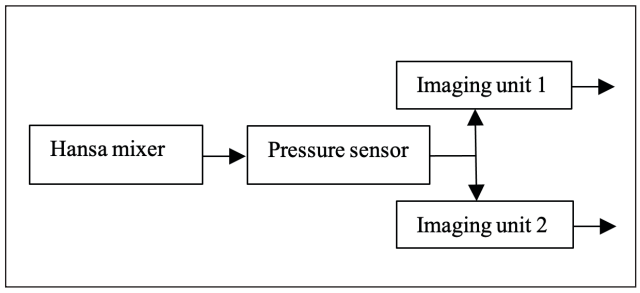
We may conclude that the presented method is able to precisely measure the size of gas bubbles. The measured bubble size distribution may be narrower than the true distribution of bubbles in foam due to the optical resolution limit for microbubbles and due to the detection algorithm limited to nearly circular shapes for large bubbles. These limitations may lower the accuracy of foam density measurement, which requires the detection of all in-focus bubbles visible in the image.

VALIDATION STUDY OF FOAM DENSITY MEASUREMENT

In this validation study, the foam density measurements of two imaging units are compared with each other and calibrated against the pressure-scaled reference foam densities obtained weighing foam samples of known volume with a digital scale. **Figure 7** presents the flow line arrangement for this study. The polyvinyl alcohol (PVOH) 6-88 solution in 3-% concentration has been utilized to produce the foam with a Hansa mixer foam generator (Hansa Industrie-Mixer Gmbh & Co.; Stuhr, Germany). Fluid viscosity is 6.0 mPas. In this study, foam flow rate is 20 kg/h through an 8-mm foam line, and the foam density varies from 100 to 270 g/L. There is a pressure sensor right before the T-junction to two imaging units. The imaging units have identical transillumination-based flow-through imaging cuvettes with a 3-mm thin and 25-mm wide rectangular flow chan-

	10 vol-% Percentile, µm	50 vol-% Percentile, µm	90 vol-% Percentile, µm
Reference range	36.3–40.2	69.5–74.9	98.9–112.1
Reference target value	38.3	72.2	105.5
Measured value	39.4	71.9	101.0

I. Accuracy assessment of size measurement: reference values and measures of volumetric size distribution of certificated glass beads.



7. Laboratory test arrangement for validation of foam density measurements.

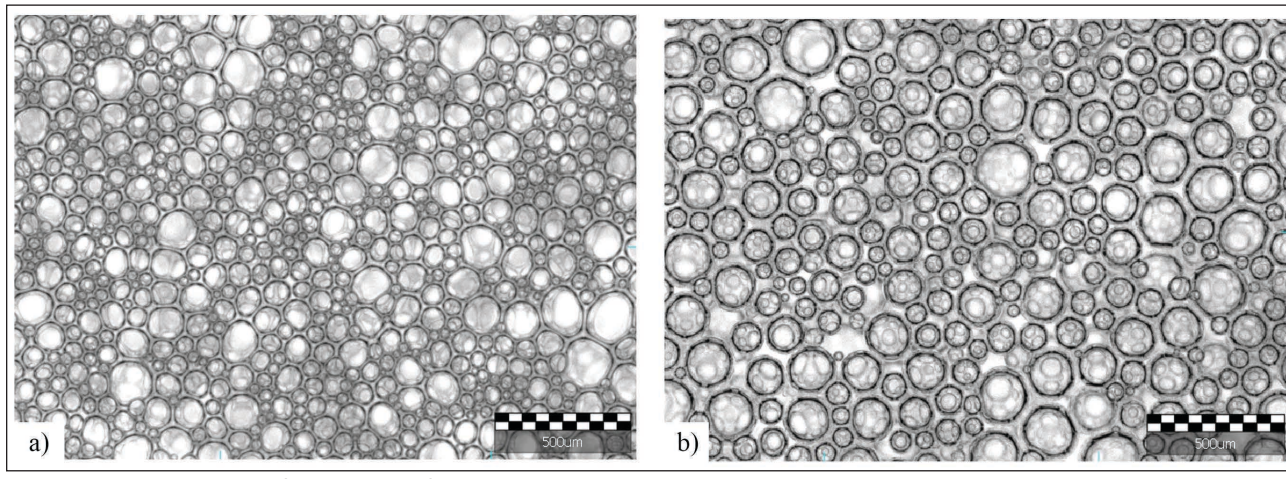
nel, but the imaging components of the units differ. It is interesting to see whether the differences in optical resolution or depth of focus of the foam images affect the measurement results.

Figure 8 presents closeup images of foam at 100 g/L and at 270 g/L densities. From the foam images in Fig. 8, one can clearly see the increase in spacing between the foam bubbles with the increase in foam density. When all bubbles are detected from the image, the remaining image regions in between the bubbles are classified as the liquid area. In this study, the computed liquid area fractions vary from 3% to 16% of the image area, and they scale linearly with the reference foam densities. The trends are the same for both measurement units. **Figure 9** presents the pressure-scaled weighted reference foam densities as a function of the measured liquid area fractions of units 1 and 2. Linear regression on the data of both units provide R^2 value of 0.99, without a noticeable difference between the measures of the two imaging units.

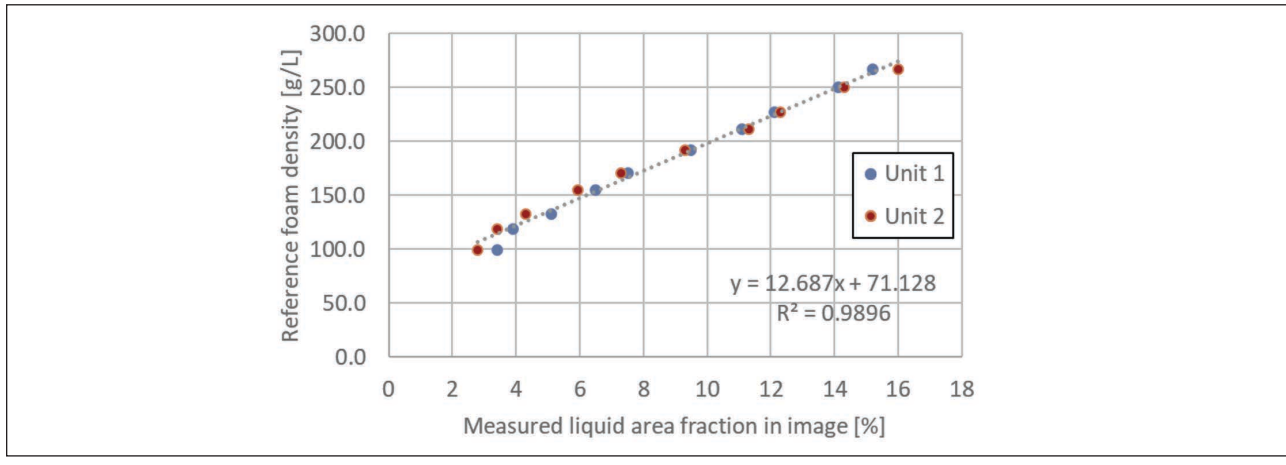
Foam density can be simply estimated based on the liquid area fraction in the image by using the result of the linear regression:

$$\rho_{fp} = 12.69 \cdot A_l' + 71.1, \quad (4)$$

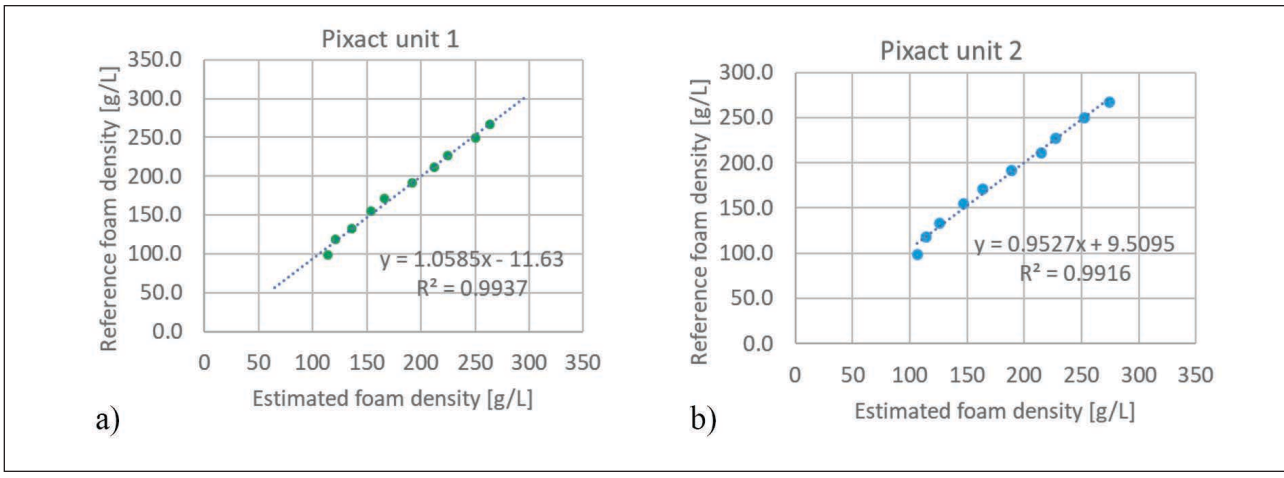
where A_l' is the liquid area fraction in the image. The estimate fails for lightweight foams below 70 g/L, because when the images are fully occupied by bubbles (A_l'=0), it gives 71.1 g/L foam density. **Figure 10** shows graphs of estimated foam densities with Eq. 5 vs. reference foam densities. Foam density estimates predict the reference foam density value very well for all other trial points, except the trial point 1 with 100 g/L, in which it overestimates the foam density by 15 g/L for unit 1 and



8. Closeup foam image at: a) 100 g/L, and b) 270 g/L.



9. Liquid area fractions in the images of units 1 and 2 vs. reference foam density in range of 100–270 g/L.



10. Estimated foam densities vs. reference foam density in range off 100–270 g/L by: a) unit 1, and b) unit 2.

7.5 g/L for unit 2. The mean error of the estimates against the reference data is 4 g/L.

We can conclude from this validation study that the optical resolution does not limit the detection of small bubbles, and the detection algorithm is also able to detect the largest gas bubbles because their shape remains nearly circular. This study may give overly optimistic results, because the studied foam was relatively homogeneous throughout the study. All other process parameters were constant, except the generated foam density. The next section of this paper presents a comparison study where foaming agent concentration, generator mixing speed, and flow rate are varied.

COMPARISON STUDY OF TRANSILLUMINATION AND FRONT LIGHT IMAGING UNIT

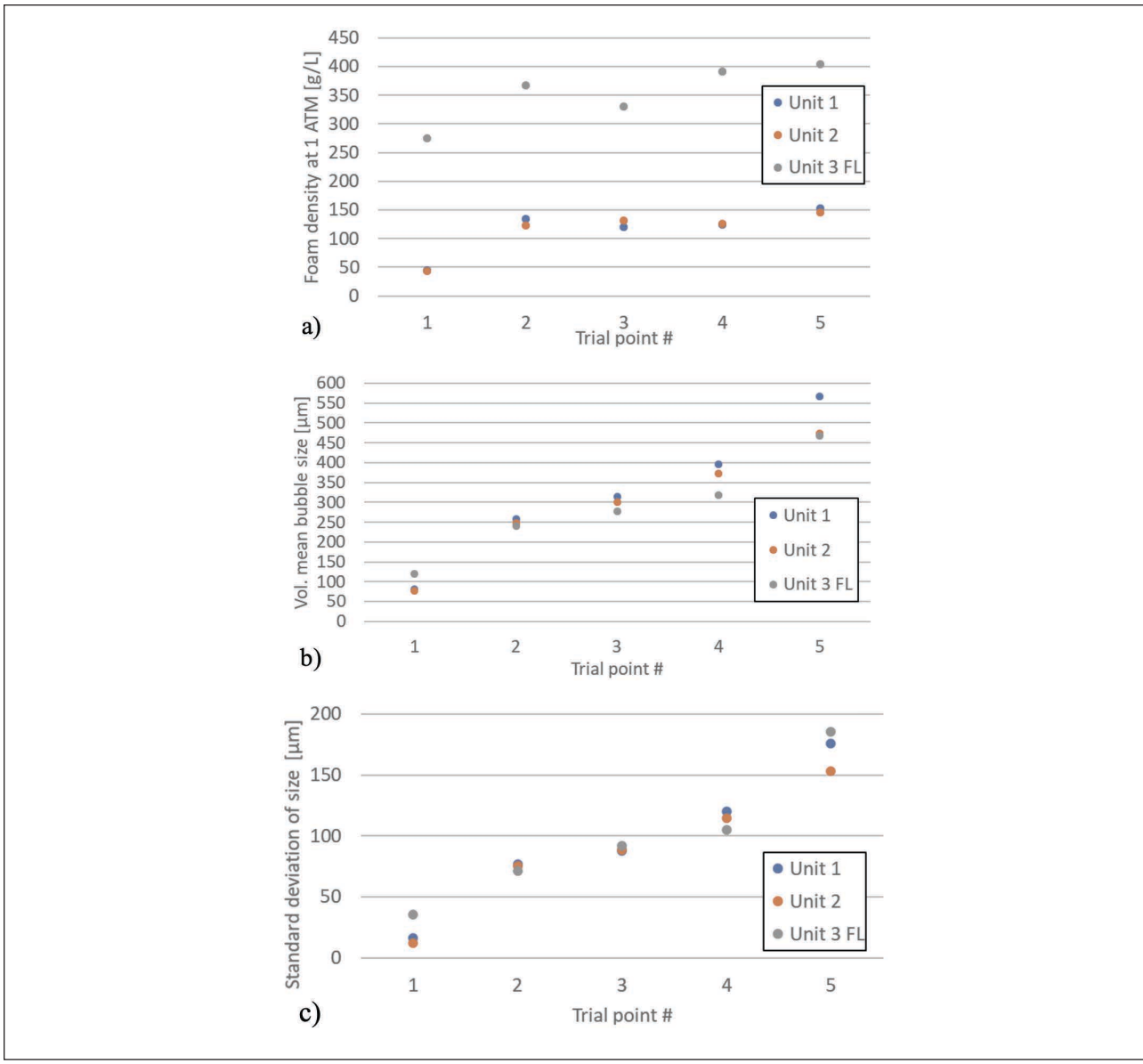
This study utilizes three imaging units in parallel. Foam travels in an 8-mm hose through unit 2, then through unit 1, and finally through the front light-illuminated unit 3 FL. Pressure sensors are located right before each measurement unit. The measured bubble sizes and foam densities are scaled to ambient pressure before performing the comparison of the measures. **Table II** lists the process parameters and the process pressure before each measurement unit during each trial point. The process conditions are more difficult for the foam measurement than in the previous validation study. In particular, the trial point 5 with a high mass flow rate is difficult for all measurement units; the elongation of bubbles affects the measurement accuracy, and isokinetic sampling of foam bubbles fails, as the bubbles on the wall do not represent the general bubble population in the channel cross-section.

Figure 11 shows the measured foam densities and volumetric mean and standard deviation of bubble size scaled to ambient pressure. Front light illumination unit "Unit 3 FL" fails to detect all bubbles in foam images, and its foam density measure is a clear overestimate in all trial points. However, the FL unit measures bubble sizes relatively well. The two transillumination-based units 1 and 2 produce bubble size results similar to each other, whereas the FL unit's size measures deviate from others by about 26 µm on average.

Figure 11c shows the measured standard deviation of bubble size distribution scaled to the ambient pressure. Standard deviation value of bubble size distribution in foam effectively reveals the foam inhomogeneity in the scale of a bubble size. All three measurement units achieve the same increasing trend between the trial points. The results highlight the differences between the trial points: bubble size and its deviation increase with a decrease in rotation

Trial Point	Mass Flow, kg/h	Foam Density, g/L	Generator Mixing, rpm	PVOH Concentration, %	p_{fp} at Unit 1, kPa	p_{fp} at Unit 2, kPa	p_{fp} at Unit 3 (FL), kPa
1	10	100	600	10	316	364	196
2	10	100	600	3	162	175	128
3	10	100	500	3	158	169	126
4	10	100	400	3	150	160	123
5	50	100	400	3	178	195	135

II. Foam process conditions in the trial points of the second validation measurements (PVOH = polyvinyl alcohol).



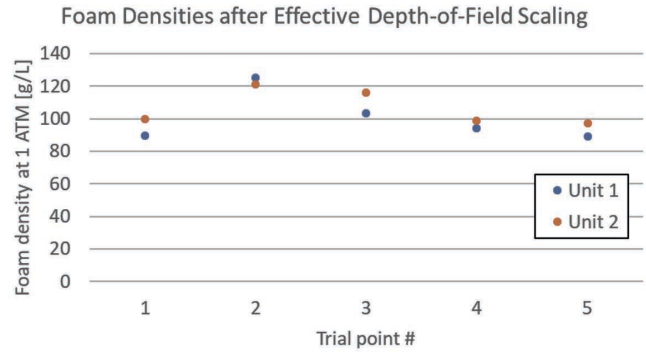
11. Graphs of a) foam densities, b) volumetric mean, and c) standard deviation of bubble size scaled to 1 ATM pressure.

speed of the mixer. The foam homogeneity also deteriorates from the heavily increased mass flow rate of the trial point 5, in which the standard deviation of bubble size exceeds 150 µm. In the validation study, the standard deviation of bubble size remained below 50 µm for all trial points, whereas in the comparison study, foam is only homogeneous at the first trial point.

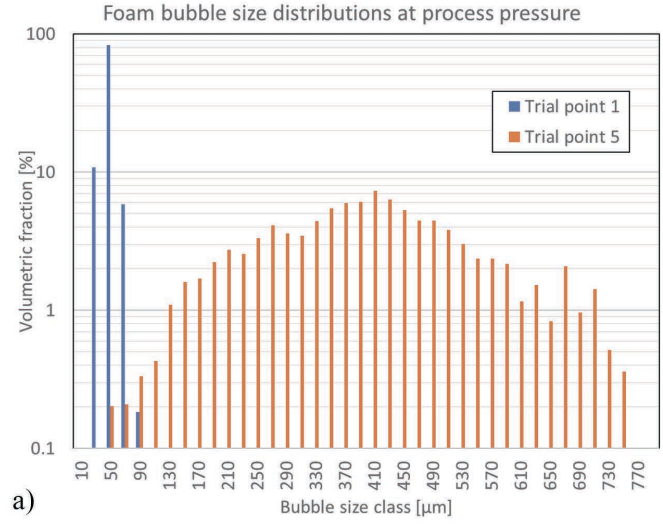
The foam densities measured by units 1 and 2 vary from 45 to 150 g/L at ambient pressure, although the reference value is 100 g/L all the time. In the process pressure, the measured foam densities vary from 125 to 250 g/L. The smallest foam density has been obtained for trial point 1, which has the highest process pressure at nearly 4 bars. At that state, the volumetric mean diameter of bubbles is only 50 µm, whereas in all other trial points, it is above 200 µm. The presented simple Eq. 5 does not apply for a wide range of foam bubble sizes. The measured liquid area fractions must be scaled with the bubble size-dependent effective depth of field. We need a dimensionless depth of field, which can be created by setting a nominal bubble diameter d_n in the numerator and the volumetric mean bubble diameter d_b in the denominator:

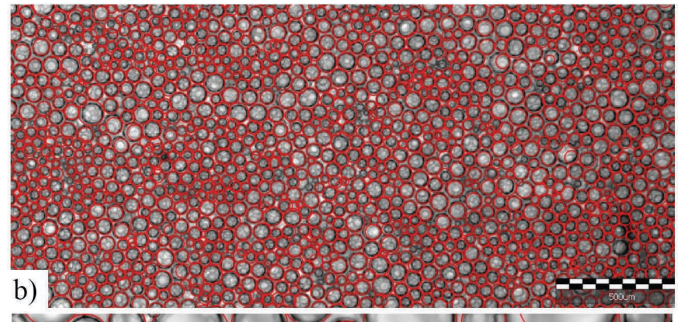
$$\rho_{fp} = 12.69 \cdot A'_l \cdot \frac{t+d_n}{t+d_b} + 71.1, \quad (5)$$

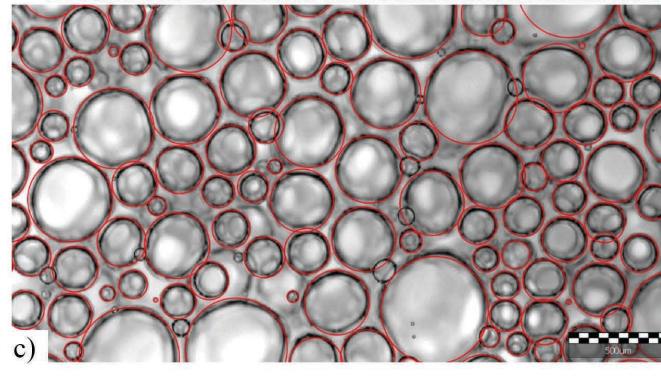
Figure 12 presents the measured foam densities after scaling the liquid area fractions with effective depth of field in each trial point. The scaling with effective depth of field reduces the mean error of foam density estimates from 37 to 10 g/L. To achieve this result, we have set the nominal bubble diameter to 200 µm and the depth of field in the image to 20 µm. The values correspond to the depth of field



12. Measured foam densities with an effective depth-of-field correction and scaling to ambient pressure.







13. a) Volumetric bubble size distributions at process pressure at TP1 and TP5; b) closeup image at TP1 with very small bubbles; and c) closeup image at TP5 with very large bubbles.

of the measuring lens, but the values depend not only on the optical setup but also on the gas bubble focus discrimination algorithm utilized. The formulation of foam density should be reviewed whenever there are changes to the measurement system.

The variety of foams in the comparison study is emphasized, comparing the volumetric bubble size distributions at process pressure at trial points 1 and 5. **Figure 13** presents the bubble size distributions and example foam images at trial points 1 and 5. At trial point 1, the volumetric bubble size distribution is nearly monodispersed; the volumetric mean bubble diameter is only 50 µm, and the standard deviation of the size distribution is only 8 µm. On the other hand, at trial point 5, the volumetric mean bubble diameter is 460 µm, and the standard deviation of bubble size is 160 µm.

CONCLUSIONS

This study quantified the accuracy of inline digital microscopy in measuring foam bubble size distribution and its standard deviation and foam density directly from the foam process. The performance has been evaluated with three studies. The first study focused on the accuracy of bubble size measurement. It showed that the automatic detection algorithm was able to detect certificated glass beads and measure their correct size, even though they were mostly overlapping with each other in the images. Accuracy assessment showed that the system measured the glass bead size distribution within the reference range of the quality audit standard.

The second study validated the camera-based foam density measurements against the reference values that were acquired by weighing a foam sample of known volume and scaling the result to process pressure. A strong linear correlation, R^2 value of 0.99, was obtained between the camera-based measures and the reference values. The second study included two imaging units, for which the foam flow was distributed through a T-junction. Both units produced the same foam density measures.

The third study compared the transillumination and front light imaging units with each other. The front light illumination approach suffered from low contrast and reflections on the surfaces of gas bubbles. It could not estimate the foam density, because the automatic bubble detection algorithm did not detect all in-focus bubbles in the front light-illuminated images. Nevertheless, the measurement of bubble size distribution was also successful in front light illumination. The comparison study showed that the bubble size-dependent depth of field must be noticed to obtain accurate estimates of foam density. After the effective depth-of-field scaling, the transillumination-based imaging units obtained foam density estimates with a mean error of 10 g/L. The measurement technique was validated for foam density range of 100–300 g/L and foam bubble size range from 10 µm to 1 mm in diameter. **TJ**

ABOUT THIS PAPER

Cite this article as:
Honkanen, M. and Eloranta, H., *TAPPI J.* 22(1): 21(2023). https://doi.org/10.32964/TJ22.1.21

DOI: https://doi.org/10.32964/TJ22.1.21

ISSN: 0734-1415

Publisher: TAPPI Press

Copyright: ©TAPPI Press 2023

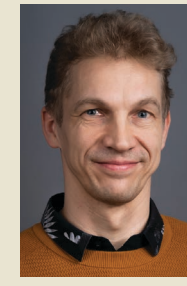
About this journal

ABOUT THE AUTHORS

This study came about because we had a research project to study real-time digital microscopy of foaming processes, and our industry partners found it important. This is the first time we have measured foam density from images, and it is a much more challenging measurement method than those we have previously used.

The most difficult aspect of this work was finding how to relate a 2D perspective projection to a 3D physical quantity such as foam density. Our most interesting finding was that we had to compensate the depth of field with the mean bubble size of foam. The other surprise was how much foam changes due to pressure change along a pipeline.

This research shows that mills might use inline microscopy for monitoring and control of their foaming processes. Currently, we are working on customer cases where foam inhomogeneity causes operational challenges, so the technique shown here has been applied in practice and is continuously developing.



Honkanen



Eloranta

Honkanen is chief technology officer and Eloranta is chief executive officer of Pixact Ltd. in Tampere, Finland. Email Honkanen at markus.honkanen@pixact.fi.

ACKNOWLEDGMENTS

This research was done in the ChemFunc project, funded in part by Business Finland. The authors wish to thank ChemFunc project parties Metsä Board, Valmet, Solenis, Sulzer, Anpap, and VTT for valuable discussion on this work and its results.

LITERATURE CITED

1. Koponen, A., Eloranta, H., Jäsberg, A., et al., *TAPPI J.* 18(8): 487(2019). https://doi.org/10.32964/TJ18.8.487.
2. Prakash, B., Jäsberg, A., and Koponen, A.I., *Annu. Trans. Nord. Rheol. Soc.* 29: 27(2021).
3. Käyhkö, J., Mutikainen, H., Peltonen, K., et al., "Gas dispersion in the oxygen delignification process," *TAPPI PEERS*, 2018, TAPPI Press, Peachtree Corners, GA, USA, p. 442.
4. Käyhkö, J., Peltonen, K., Mutikainen, H., et al., *TAPPI J.* 20(5): 321(2021). https://doi.org/10.32964/TJ20.5.321.
5. Kroezen, A.B.J. and Groot Wassink, J., *J. Soc. Dyers Colour.* 103(11): 386(1987). https://doi.org/10.1111/j.1478-4408.1987.tb01090.x.
6. Kroezen, A.B.J., Groot Wassink, J., and Schipper, C.A.C., *J. Soc. Dyers Colour.* 104(10): 400(1988). https://doi.org/10.1111/j.1478-4408.1988.tb01138.x.
7. Eloranta, H., Honkanen, M., and Myers, C., "Online measurements of sugar crystallization campaign with a portable non-intrusive instrument," *Sugar Ind. Technol. Annu. Meet., 78th*, Sugar Industry Technologists, Myrtle Beach, SC, USA, 2019. Available [Online] https://www.pixact.fi/_files/ugd/80d217_be99c360dffc45c79af6c-122fa20944a.pdf <12Dec2022>.
8. Lecuona, A., Sosa, P.A., Rodriguez, P.A., et al., *Meas. Sci. Technol.* 11(8): 1152(2000). https://doi.org/10.1088/0957-0233/11/8/309.
9. Overby, D.R. and Johnson, M., *J. Microsc.* 220(3): 176(2005). https://doi.org/10.1111/j.1365-2818.2005.01520.x.
10. Malvern Panalytical, "MasterSizer 2000 Hydro 2000M/MU Quality Audit Standard CCM0062-01-EN," Malvern Panalytical, Malvern, UK, 2021. Available [Online] https://www.malvernpanalytical.com/en/assets/CCM0062-01-QAS4002-EN%20Hydro%202000MMU%20%28SECURED%29_tcm50-60202.pdf <12Dec2022>.
11. Junker, B., Maciejak, W., Darnell, B., et al., *Bioprocess Biosyst. Eng.* 30: 313(2007). https://doi.org/10.1007/s00449-007-0127-y.